



# **FLEXIBLE GELSEIGHT SENSOR DESIGN FOR TISSUE HARDNESS ESTIMATION DURING ENDOSCOPIC SURGERY**

**BN5101- Biomedical Engineering Systems -Final report**

Module Facilitator: Prof. **Ren Hongliang**

KEERTANA VINOD RAM – A0213606N  
LONG KAI – A0219012W  
ADITI POHEKAR–A0219106M

## Contents

Flexible GelSight Sensor Design for Estimation of Tissue Hardness During Endoscopic Surgery .....	1
Keywords .....	1
Abstract.....	1
1. Introduction.....	1
2. Related works.....	2
2.1 Hardness Sensor.....	2
2.2 Shaft design inspired by origami .....	5
2.2.1 Origami pattern .....	5
2.2.2 Actuation mechanisms .....	9
3 Approach (4A) .....	10
3.1 Main block diagram and explanation (Architecture) .....	10
3.2 Optical perception (Awareness).....	10
3.3 Telescopic shaft (Actuator).....	11
3.3.1 Strain Visualization.....	11
3.3.2 Degrees of Freedom (DOFs).....	12
3.4 Image processing algorithm (AI) .....	13
4 Method .....	14
4.1 Data collection .....	14
4.1.1 Shape classification.....	14
4.1.2 Force estimation.....	14
4.2 Data Processing.....	15
4.2.1 Shape classification.....	15
4.2.2 Force estimation.....	16
4 Results.....	17
5 Conclusion .....	18
6 Limitations and Future Work.....	18
References.....	19

## List of figures

Figure 1: Basic origami concepts [17] .....	5
Figure 2: a) Crease pattern; b) paper model.....	7
Figure 3: a) crease pattern; b) paper model.....	7
Figure 4: a) Crease pattern; b) Paper model .....	8
Figure 5: a) creases to fold an origami segment, b) folded segment, c) assembled tower when extended, d) assembled tower when fully contracted, and e) assembled tower when bent. [24].....	8
Figure 6: a) Final shape of origami magic ball cylinder after assembly; b) Parameters that define the bending motion of the design [17] .....	8
Figure 7: Telescopic hardness sensor.....	10
Figure 8: Information flow of the hardness sensor .....	10
Figure 9: a) Camera with LED light source; b) LEDs in the middle of the origami sleeve.....	11
Figure 10: a) Accordion pattern based bellow; b) Diagonal pattern based collapsible paper column..	11
Figure 11: Engineering strain for a) origami square bellows and b) collapsible paper column at fold percentage = 52% .....	12
Figure 12 : Crease pattern for a) Accordion pattern, b) Diagonal pattern .....	12
Figure 13: Image processing algorithm diagram .....	13
Figure 14: a) Bellow prototype, b) Paper column prototype.....	14
Figure 15: 3-D printed shapes.....	14
Figure 16: Shape classification images .....	14
Figure 17: Setup of force estimation.....	14
Figure 18: Force estimation images .....	15
Figure 19: Algorithm for shape classification.....	15
Figure 20: Graph of training and validation accuracy of Shape classification CNN model .....	15
Figure 21: Algorithm for force estimation .....	16
Figure 22: Graph of training and validation accuracy of Force classification CNN model.....	16
Figure 23: Shape classification data collected by bellow and paper column structures .....	17
Figure 24: Shape classification accuracy of bellow and paper column for four shapes .....	17

# Flexible GelSight Sensor Design for Estimation of Tissue Hardness During Endoscopic Surgery

## Keywords

GelSight sensor, elastomer, camera, tissue hardness, origami, actuation, automation, architecture

## Abstract

The tactile properties of a tissue such as hardness, texture, shape, are important for surgical procedures. While this information is obtained effortlessly during an open surgery, in a minimally invasive endoscopic surgery this is compromised. To address this issue there are several developments in the tactile sensing field but lack the flexibility required for use in endoscopy. This proposal discusses the implementation of pliability using two different origami structures with tactile sensing ability of a traditional GelSight sensor for shape classification and force estimation. The shape classification is done using the intensity changes through the transparent elastomer and the force estimation is done by additionally adding markers on the surface of the sensor. Retaining the tactile sensing ability, the two origami structures square origami bellow and collapsible paper column are compared for their stability and compliance to the application. The collapsible paper column is concluded to have higher stability and greater application. The model is then verified for shape classification and force estimation by processing data collected from these prototypes for classification of 4 different shapes and force estimation for 5 different classes.

## 1. Introduction

Endoscopy refers to a minimally invasive procedure in which a slender tubular optical instrument (endoscope) is inserted inside the body to examine internal organs. Endoscopic procedures can be performed by inserting the endoscopic tubes into the body either through a natural orifice like nostril, mouth, anus etc. or through small incisions[1],[2]. There are different kinds of endoscopic procedures based on the path followed by the endoscope. Some examples are Bronchoscopy, Colonoscopy, and Gastrosocopy etc.[3]. This procedure caters to various needs such as diagnosis, tumor removal, tissue biopsy, stent placements etc. Surgery is one of the major applications of endoscopic setup. Due to its minimally invasive nature, use of this technology in surgery offers a lot of advantages, like relatively low risk of infection, faster recovery of the patients and less scarring.

However, endoscopic minimally invasive surgery also has certain challenges as compared to the traditional methods. First is that tactile sensibility of the operating environment is compromised [4], [5]. Tactile feedback is very important during tool-tissue interaction because of two major reasons. Firstly, it enables the surgeon to apply force in an appropriate manner, so as to prevent any damage to the healthy tissues, thus ensuring safety of the procedure. Another reason is that it helps in the characterization of the contacted tissues [6]–[8]. Usually, during open surgeries this information can be collected in the most intuitive and effective way using human finger. But in endoscopic surgery this cannot be achieved naturally. Hence, there is a need for artificial tactile feedback. Tactile feedback is also important because properties like hardness, texture and shape of the site of interest are an important indicator of tissue's health. For instance, malignant tumors are significantly harder than normal tissues [9]. In this context, use of a tactile sensor in the system can add tactile capability to the system and improve perception of the operating environment.

Another major challenge in endoscopic surgery is the constraint space of the operating environment. The entry point is usually small in the form of a natural orifice or a key-hole incision. Also, the track followed by the endoscope is narrow and tortuous. Therefore, the shaft design is expected to be slender and highly flexible. The papers [10], [11] show that structural stability can be obtained along with addition of flexibility with the use of origami inspired shafts.

The aim of the project is to make contribution to propose a model for a telescopic tactile sensor which can perform shape classification and force estimation. The tactile properties are obtained along with the added structural flexibility and dexterity. This can eventually be used for measurement of tissue hardness. The two origami designs are compared, and the final model is assumed to have a higher adaptability to endoscopic related biomedical applications. The proposal integrates a traditional hardness sensor with an origami sleeve design to introduce flexibility. Finally, the shape classification and force estimation results are obtained by training a CNN model and the training and validation accuracy of the same are discussed in this proposal.

## 2. Related works

### 2.1 Hardness Sensor

Some of the earlier works related to tactile sensing are discussed in this section. The modified GelSight sensor in [12] discusses the measurement of the hardness of objects without restrictions in force applied and Surface geometry. It worked on the principle of image processing of image captured from the elastomeric material to obtain brightness and radius values to determine hardness. The estimation was done only on silicone spherical shapes which indicated limitation in shape of sample.[12] . A methodology was proposed to determine the topography of tissues and different properties of tissues such as tumors. This paper mainly involves the usage of deep learning and machine. learning models like General Adversarial Network (GAN) and Convolutional Neural Network (CNN). The distance between the camera and sensing material was comparatively big and cumbersome in its architecture [13]. Another model was proposed for estimation of hardness using a tactile sensor based on frequency shift during the vibration of piezoelectric element. The methodology uses a mathematical model to determine the frequency shift and uses a one-way ANOVA model and multiple regression model for statistical data analysis. This paper indicates how different tissue compositions could indicate a disease possibility. The only disadvantage being the invasiveness and the paper indicates further miniaturization of size [14]. Shogo Okamoto et al. came up with a soft tactile sensor that gives the estimate of characteristics like roughness, friction, and hardness of samples. The experiment also involves calculation of young's moduli of 3 samples using a strain gauge. This method was successful in obtaining sample's spatial wavelength and was also the first tactile sensing unit to give a real time quick sensing information [6]. The model by Mike Lambeta et al. is the most recent development in the tactile sensing devices. It uses machine learning models for training. Feature maps are obtained from the images captured in the camera which are then encoded to obtain positions and intensity details [9]. The figures in [Table 1](#) show the design and appearance of different hardness sensors. Below we make a detailed comparison of the content of these researchers in main framework, Paradigm, gaps and so on, as shown in [Table 2](#).With these developments in the field of tactile sensing, our proposal aims at increasing the flexibility of a tactile sensor along with usage of an endoscope camera set-up with appropriate illumination to obtain image with sufficient resolution and clarity.

Table 1: Structure diagram of different hardness sensor





GelSight sensor [12]	Depth estimation with haptic vision [13]	Human Finger mimetic sensor [6]	Digit [9]
			

Table 2: Comparison of hardness sensors with different characteristics

Author/Year	Topic	Main Framework	Paradigm	Findings	Gaps
Wenzhen Yuan - 2016[12]	<ul style="list-style-type: none"> <li>Estimating object Hardness with a Gel sight sensor</li> <li>Estimation of hardness of objects without restrictions in force applied and Surface geometry.</li> </ul>	<ul style="list-style-type: none"> <li>Image processing of tactile images captured by camera.</li> <li>Implements mathematical model for calculation of hardness.</li> </ul>	<ul style="list-style-type: none"> <li>Using a Gel Sight sensor for sensing and capturing the image with illumination.</li> <li>Brightness of the image indicates the surface normal and shape characteristics.</li> <li>The markers are placed on the elastomeric material which is used to detect pressing force.</li> </ul>	<ul style="list-style-type: none"> <li>Gel sight Sensor is a good miniaturized product for detection of shape/ texture/ Hardness characteristics.</li> <li>The detection of hardness is done without Heightmap.</li> </ul>	<ul style="list-style-type: none"> <li>The experiment is done on Silicone spherical samples of different sizes; hence it is not valid for different shapes and objects.</li> </ul>
Lee Jia yi, Lalithkumar Seenivasan,	<ul style="list-style-type: none"> <li>Deep Learning Based Depth Mapping, Classification and</li> </ul>	<ul style="list-style-type: none"> <li>General Adversarial Network(GAN) for Output Depth</li> </ul>	<ul style="list-style-type: none"> <li>Depth estimation, shape classification and force estimation of test subject is carried out.</li> </ul>	<ul style="list-style-type: none"> <li>-The three tasks i.e. Depth estimation, shape classification and force estimation, through the</li> </ul>	<ul style="list-style-type: none"> <li>The distance between the camera and object is comparatively big and can be minimized.</li> </ul>

<b>Kirthika Kumar and Dr Ren Hongliang [13]</b>	<ul style="list-style-type: none"> <li>Force Estimation For Haptic Vision.</li> <li>Estimation of topography of human tissues such as tumors.</li> </ul>	<ul style="list-style-type: none"> <li>Map Convolutional Neural Network (CNN) for Pressure map</li> </ul>	<ul style="list-style-type: none"> <li>The Input image and the output depth map are converted to grey image, further giving the probability of shapes.</li> <li>- The same when input to a CNN model for force estimation gives a pressure map</li> </ul>	<ul style="list-style-type: none"> <li>proposed experimental setup, can be used to estimate the topography of human tissues such as tumors</li> </ul>	<ul style="list-style-type: none"> <li>Flexibility of the sensor can be improved, as it is invasive.</li> </ul>
<b>Eklund,A. Bergh,O.A. Lindahl - 1999 [14]</b>	<ul style="list-style-type: none"> <li>A catheter tactile sensor for measuring hardness of soft tissue</li> </ul>	<ul style="list-style-type: none"> <li>Mathematical model is used to determine the frequency shift.</li> <li>One way ANOVA model and multiple regression model is used for statistical data analysis.</li> </ul>	<ul style="list-style-type: none"> <li>- Measurement of hardness using a tactile sensor based on frequency shift during the vibration of piezoelectric element.</li> </ul>	<ul style="list-style-type: none"> <li>The hardness of a tissue depends on the particular tissue composition. A variation in the tissue composition indicates disease possibility.</li> <li>- The catheter tip tactile sensor was successful in determining tissue hardness for diagnosis of prostate cancer</li> </ul>	<ul style="list-style-type: none"> <li>The method is invasive. Further minimization of size could be done.</li> <li>The experiment is particular for prostate tissue.</li> </ul>
<b>Shogo Okamoto - 2016[6]</b>	<ul style="list-style-type: none"> <li>Real-time Estimation of Touch Feeling Factors Using Human Finger Mimetic Tactile Sensors</li> </ul>	<ul style="list-style-type: none"> <li>Vibrational frequency determination using short time Fourier transform</li> </ul>	<ul style="list-style-type: none"> <li>It is around soft tactile sensor that estimates roughness, friction and hardness.</li> <li>- Young's moduli of three different samples is calculated using a strain gauge.</li> </ul>	<ul style="list-style-type: none"> <li>The method was suitable for measuring different touch parameters and also the object's spatial wavelength.</li> <li>- Real-time quick sensing of tactile factors is obtained.</li> </ul>	<ul style="list-style-type: none"> <li>the load or the force applied is controlled.</li> <li>The sample shapes are limited.</li> </ul>
<b>Mike Lambeta- 2020[9]</b>	<ul style="list-style-type: none"> <li>DIGIT: A Novel Design for a Low-Cost Compact High-Resolution Tactile Sensor with Application to In-Hand Manipulation</li> </ul>	<ul style="list-style-type: none"> <li>Feature map, encoder and learned dynamics model for training</li> </ul>	<ul style="list-style-type: none"> <li>Precisely sensing contact forces.</li> <li>Position of object is determined, and feature map is obtained. Robot is trained using a learned dynamics model.</li> </ul>	<ul style="list-style-type: none"> <li>DIGIT provides rich, high-resolution tactile readings.</li> <li>The capabilities of the sensor are demonstrated using marble movement</li> </ul>	<ul style="list-style-type: none"> <li>Minimizing the size of the sensor.</li> <li>Sensing of curved surfaces.</li> </ul>



## 2.2 Shaft design inspired by origami

Origami-inspired robotics refers to the use of origami patterns, built using different materials (for example acrylic, vero etc.), for various applications like manipulation, locomotion, gripping etc. This set up has many advantages over traditional systems. For instance, the part can be built in 2-D and folded to 3-D, making the manufacturing process simpler. Secondly, the size of the structure can be reduced to a great extent, as origami patterns are size invariant. Also, it offers high degrees of freedom. Therefore, this concept has been explored for this project. In general, origami-inspired robotics consists of two parts 1) **origami pattern** and 2) **actuation mechanism** [15].

### 2.2.1 Origami pattern

This section explores basic geometry involved in designing an origami structure and its use in various engineering applications. As shown in [Figure 1](#), following are some basic concept of origami [16]:

- **Crease** – Folds on sheet/ material
- **Mountain** – Creases that are convex
- **Valley** – Creases that are concave
- **Faces** – Flat surfaces enclosed by creases
- **Folding angle** – Angle at which any crease is folded
- **Radius of curvature** – Curvature of the fold, since any material will have a finite thickness, which will cause the fold to have a certain curvature.

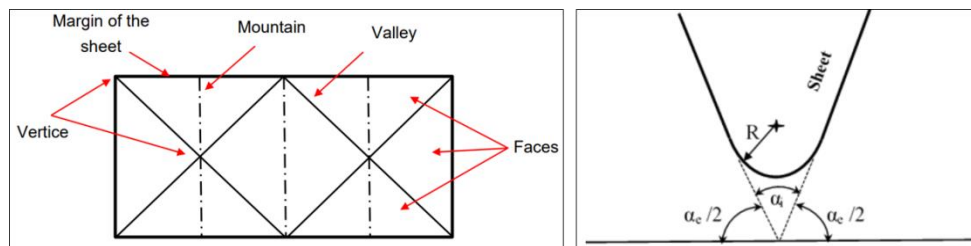


Figure 1: Basic origami concepts [17]

Origami structures can be broadly classified into two types:

- **Tessellation Origami** – Structure made of a single sheet. It consists of a specific periodic geometrical pattern with creases as its edges (unit cell). Each unit cell consists of certain constant parameters, which don't change during the folding process, and some variable parameters, which are altered during the folding process. For example: Miura pattern, Water bomb pattern, accordion pattern etc.
- **Modular Origami** – Structure made of origami segments linked to each other. For example: Twisted tower.

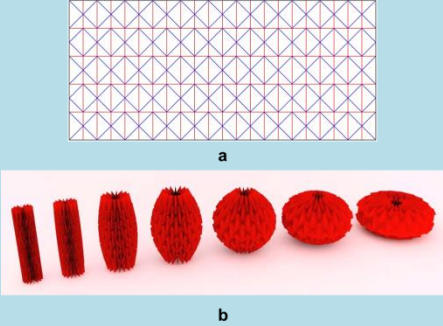
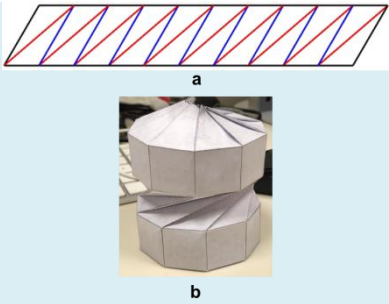
There is plenty of literature available demonstrating the use of different origami structures for various applications. The twisted tower structure, is highly flexible and also can be analyzed by using rigid body dynamics [18]. Origami magic ball based cylinder proposed in [19] is a modular structure with magic ball/ water bomb as a single unit, is again highly flexible. However, cumbersomeness of the two structures due to the multiple folding creases is a major drawback. Chen et al. discussed diagonal pattern based twisted paper column, which is a single sheet structure which offers linear displacement in the vertical direction with a twisted opening and closing action [20]. Butler et al. proposed accordion pattern based origami bellows structure, which is again a single sheet structure, but assembled in a way to offer three DOFs [21]. Thus, it's simple and highly flexible at the same time. Hence, several origami-inspired structures are evaluated on the basis of simplicity and flexibility, in order to design a suitable structure for the shaft of the proposed tactile sensor.

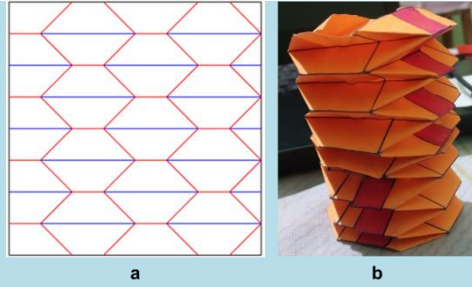
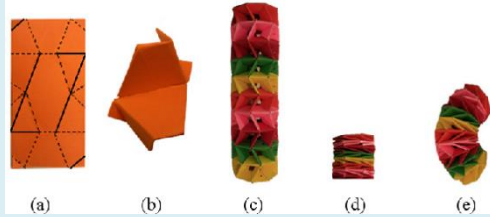
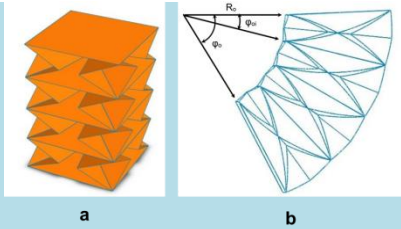
A more detailed description of the various origami patterns is presented in the [Table 1](#)



Table 3: Comparison of origami-inspired patterns

Structures	Type	Unit Cell	Motion Description
Water bomb/ Origami magic ball [22]	Tessellation	Six isosceles triangles connected at their heads to create a square shape. Each unit cell is folded into two mountain and four valley creases.	<ul style="list-style-type: none"> <li>▪ Elongation and compression.</li> <li>▪ Variable parameters: <ul style="list-style-type: none"> <li>- Side folding distances = <math>x_{fr}</math> and <math>x_{fl}</math></li> <li>- Width folding distances = <math>y_{fr}</math> and <math>y_{fl}</math></li> <li>- Height = <math>h_b</math></li> <li>- Dihedral angles = <math>\gamma_{br}</math> and <math>\gamma_{bl}</math></li> <li>- Projection angle = <math>\alpha_b</math></li> </ul> </li> <li>▪ Constant parameters: The unit cell has just one constant parameter, which is the length of the side of the square (<math>a_b</math>)</li> </ul>
Diagonal Pattern [23]	Tessellation	Parallelogram	<ul style="list-style-type: none"> <li>▪ The cylinder made using this pattern rotates and folds with torsional buckling</li> </ul>
Accordion pattern [16]	Tessellation	2 trapeziums connected through the longer one among the parallel sides.	<ul style="list-style-type: none"> <li>▪ This pattern can be assembled to form <b>origami bellows</b>.</li> <li>▪ Origami bellows can be compressed and expanded along the vertical axis. It can also be bent within a limited range. However, large bending can be obtained if it is used a unit module in a modular origami structure.</li> </ul>
Twisted Tower [24]	Modular	16 identical origami segments linked to form an octagonal pattern. Each octagonal is stacked to form a tower.	<ul style="list-style-type: none"> <li>▪ Elongation, compression and bending motion</li> </ul>
Origami Magic ball [17]	Modular	More appropriate for manipulation applications	<ul style="list-style-type: none"> <li>▪ Elongation, compression and bending motion</li> <li>▪ Bending angle, <math>\phi_0 = \frac{\eta y_{f1}}{R_0}</math></li> </ul>

Structure	DOF	Pros and cons	Icon
Origami magic ball [22]	1	<ul style="list-style-type: none"> <li>Pros: Single sheet structure</li> <li>Cons: Actuation could be difficult because of the change in radius</li> </ul>	 <p>Figure 2: a) Crease pattern; b) paper model</p>
Diagonal Pattern based collapsible paper column [23]	1	<ul style="list-style-type: none"> <li>Pros: Single sheet structure</li> <li>Cons: Complicated helical movement</li> </ul>	 <p>Figure 3: a) crease pattern; b) paper model</p>

<p><b>Accordion pattern/ Square origami bellows</b> [16]</p>	1	<ul style="list-style-type: none"> <li>Pros: Single sheet structure</li> <li>Cons: Assembly can be slightly complicated</li> </ul>	 <p><b>Figure 4: a) Crease pattern; b) Paper model</b></p>
<p><b>Twisted Tower</b> [24]</p>	3	<ul style="list-style-type: none"> <li>Pros: Conventional rigid body dynamics can be used for this, as the structure resembles rigid-body like motion</li> <li>Cons: Cumbersome, complicated</li> </ul>	 <p><b>Figure 5: a) creases to fold an origami segment, b) folded segment, c) assembled tower when extended, d) assembled tower when fully contracted, and e) assembled tower when bent. [24]</b></p>
<p><b>Origami Magic ball cylinder</b> [17]</p>	3	<ul style="list-style-type: none"> <li>Pros: High degrees of freedom</li> <li>Cons: Complicated</li> </ul>	 <p><b>Figure 6: a) Final shape of origami magic ball cylinder after assembly; b) Parameters that define the bending motion of the design [17]</b></p>

### 2.2.2 Actuation mechanisms

There are two types of actuation mechanisms as discussed below:

- 1. External Actuators** – In an externally actuated system the actuator lies outside the origami structure. Force is transmitted using a force transmission system, for example, cables, strings, chains etc. This type typically provides more actuation force. This type is more suitable for manipulation structures like origami-based grasper etc.
- 2. Embedded Actuators** – In an embedded actuation system the actuator is situated inside the origami structure. This kind provides less actuation force. However, this type is more suitable for self-folding structures because self-folding process used in locomotion applications requires many hinges to bend at certain angles, which would require too many external actuators. Hence, embedded actuators placed at each hinge forms a simple and more effective solution.

Some of the common actuation mechanisms, used for origami structures, are discussed in [Table 4](#)

**Table 4: Common actuation mechanisms used for origami structures**

Type	Name	Description of mechanism	Materials
External Actuation	Electrical motor	Force transmitted through motors which leads to the pulling and pushing of transmission systems like using cables, strings, chains etc., which causes expansion, contractions and bending of the shaft	Servo motor + pulley + cable [24]
	Pneumatic Actuation	Movement generated through deformation caused by compression and expansion of gas inside a soft material	Ecoflex [25], [26]
Embedded Actuation	Thermal Actuation	Movement takes place due to expansion and contraction of material caused due to heating. Materials with high thermal expansion coefficient are used as actuators	paperboard + polyimide film [27] TiNi SMA foil [28] PVC + aluminized polyester [29] paper + water-based ink + carbon-based ink [30]
	Electrical actuation	Altering of electric field causes bending of the actuator, which leads to movement in the origami structure	Polypyrrole films, polydimethylsiloxane (PDMS) [31]
	Photo actuation	Actuation generated by illumination through two mechanisms: 1. Heat generated 2. Change in microstructure of the actuator	Pentaerythritol tetra(3-mercaptopropionate) (PETMP) [32] GaAs [33]
	Cell force based actuation	Cell traction force (CTF), which is an intercellular force is used to generate motion. This can be used for designing biocompatible micro-robots, drug carriers, biological stent grafts etc.	3T3 cells or BAOSMCs [34]

### 3 Approach (4A)

#### 3.1 Main block diagram and explanation (Architecture)

Figure 7 represents the various components of the telescopic harness sensor. The top layer possesses the incision for endoscopic camera. The intermediate shaft is composed of adjustable flexible origami sleeve with additional illumination set-up with Light-emitting diodes (LED). The bottom layer consists of stretchable elastomeric membrane with optical markers.

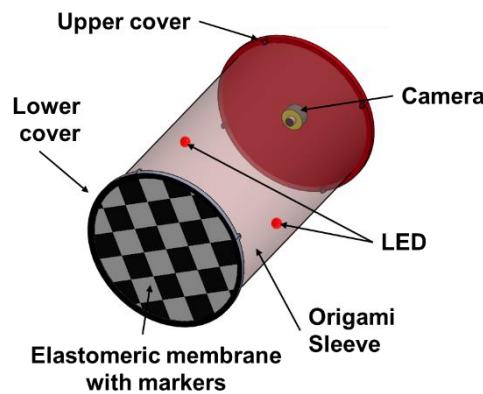


Figure 7: Telescopic hardness sensor

Figure 8 shows the functional flow of Figure 8the hardness sensor. First, the sample encounters the elastomeric membrane attached to the lower cover of model. The markers placed on the elastomer play a key role in contact force estimation. This is because in this case instead of measuring the contact force directly, optical information about the displacement of markers is used to calculate the force exerted. An optical source, which in this case is either the light source attached to the camera or LEDs attached on the origami sleeve, is used to illuminate the target. This ensures that the images are of good quality and contain maximum information about the boundaries of the target sample and position of the markers. Next component is the origami sleeve, which has a bistable structure and is expected to be in a fully open state during the measurements. The maximum force that can be exerted on the sample without deformation in the origami is 1N in the current architecture. After this the miniature endoscopic camera is used to capture the image. Finally, the image is processed to derive information about the shape of the target sample and the force exerted.



Figure 8: Information flow of the hardness sensor

#### 3.2 Optical perception (Awareness)

The optical perception (awareness) deals with capturing images of the elastomeric material. The most important aspect for perception of good quality images is illumination. In order to obtain the ideal illumination, the light source should meet the requirements of sufficient and adjustable brightness and stay inert to the surrounding light. To satisfy these criteria, we used two illumination methods, one is the adjustable light source that comes with the endoscope placed opposite to the elastomer (Figure 9a), the other is LEDs of two different wavelengths placed at the lateral edges of the sensor (Figure 9b). These LEDs are used to avoid overexposure of vertical light from the endoscope. The dataset was

collected with minimum illumination from endoscope and maximum illumination from the LEDs power by a 2V DC power supply. The elastomeric material used is the second important aspect of awareness. The material used is ecoflex which is extensively used in tactile applications because of its low viscosity and high stretchability. The elastomeric material covers up to an area of 7 cm<sup>2</sup>. The material is then marked with black industrial paint markers.

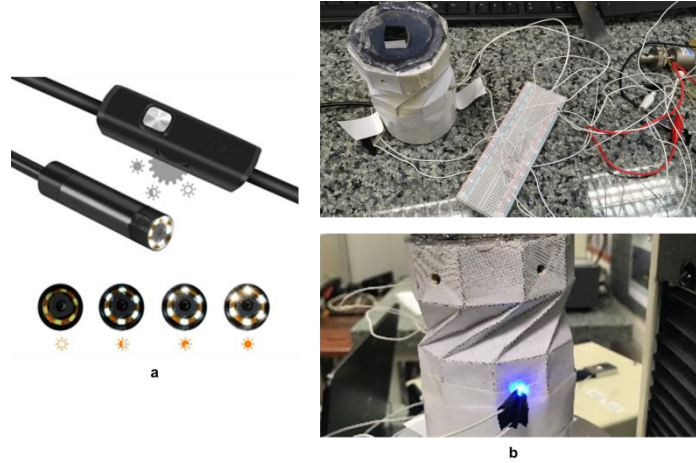


Figure 9: a) Camera with LED light source; b) LEDs in the middle of the origami sleeve

### 3.3 Telescopic shaft (Actuator)

For the current application, the origami structures used are single sheet structures, i) accordion pattern based square bellows (Figure 10a) and ii) diagonal pattern based collapsible paper column (Figure 10b), due to the simplicity and slickness these structures offer.

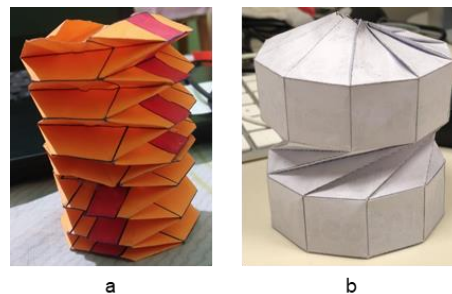


Figure 10: a) Accordion pattern based bellow; b) Diagonal pattern based collapsible paper column

Currently, for the scope of this project we have not implemented any automated actuation mechanism and origami structure is being moved manually. However, the structures proposed can be miniaturized and actuated using the actuation mechanisms discussed in Table 4. The two structures are compared on three aspects, viz. strain visualization, degrees of freedom and pattern recognition accuracy.

#### 3.3.1 Strain Visualization

Strain visualization for the two structures is done using [origamisimulator.org](http://origamisimulator.org) [35]. The simulator approximates the engineering strain/ Cauchy strain across the surface of the origami structure by measuring the displacement of the axial constraints. The engineering strain  $\epsilon$  is defined in Equation 1 [36]

$$\epsilon = \frac{l - l_0}{l_0}$$

Equation 1

Here  $l$  is the length of the beam, and  $l_0$  is the nominal length of the beam.

Engineering strain at a node with  $N$  beams is defined in Equation 2 [36]

$$\epsilon_{node} = \frac{1}{N} \sum_{i=1}^N \frac{|\Delta l_i|}{l_i}$$

Equation 2

It is calculated by averaging the absolute value of the strain contribution from each beam.

From the strain visualization simulation performed using Amanda Ghassaei's origami simulator (Figure 11), it can be said that for the fold percentage, collapsible paper column displays more strain values. Therefore, it can be said that for the same amount folding collapsible paper column can give more displacement as compared to diagonal pattern.

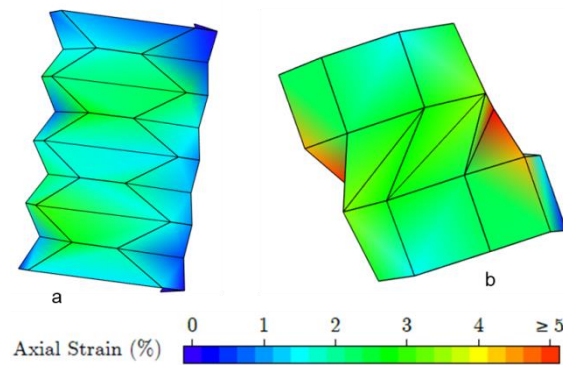


Figure 11: Engineering strain for a) origami square bellows and b) collapsible paper column at fold percentage = 52%

### 3.3.2 Degrees of Freedom (DOFs)

The DOFs mentioned for various origami structures described in Table 3 are considering an ideal case scenario where each rigid face has uniform motion. However, in real life this may not be the default case. In such a situation, more number of creases could add more uncertainty to motion of the structure. Thus, in this section we have tried to evaluate the number of DOFs of both the origami structures.

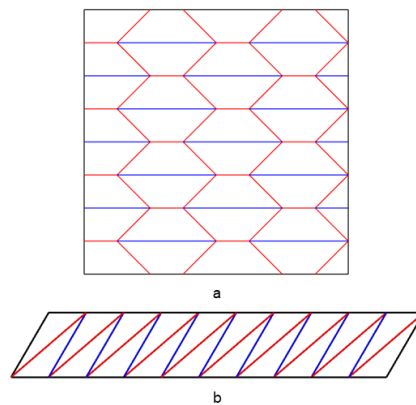


Figure 12 : Crease pattern for a) Accordion pattern, b) Diagonal pattern



The degrees of freedom of a 3-D origami can be defined as [37]:

$$DOF = N_{E_0} - 3N_L - 3$$

Equation 3

Where,  $N_{E_0}$  is number of edges on the boundary and  $N_L$  number of holes[38]. By referring the crease patterns for both the structure (Figure 12), the DOFs are calculated for the structures using Equation 3

Pattern	Accordion pattern based bellows	Diagonal pattern based collapsible column
$N_{E_0}$	20	11
$N_L$	1	1
DOF	14	5

It can be observed that collapsible paper column has less number of creases as well as less number of DOFs. Therefore, paper column is theoretically a more stable structure.

### 3.4 Image processing algorithm (AI)

Once the image is captured by the camera, it must be processed to obtain the details regarding tissue hardness. The beauty of image processing enables us to obtain properties of the tissue from preliminary values of intensity and marker area expansion in the image captured. Here, we use the technique of obtaining the surface normal characteristics and shape characteristics of the sample by observing the brightness/intensity change in the image [12]. The brightness change is directly proportional to the hardness of the surface, because as observed in [12] the brightness in the image increases for harder objects when force is applied. Thus, the intensity value is an important parameter obtained from the image captured. We also add a marker field on the surface of the elastomeric material so as to observe the surface indentation of the elastomer when force is applied on the sample. The expansion in the marker field is directly proportional to the contact force between the elastomeric material and the sample. It is learned that harder objects increase the indentation.

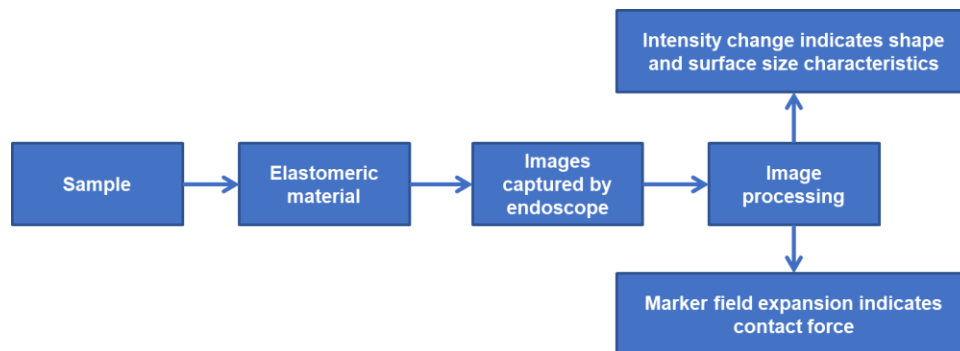


Figure 13: Image processing algorithm diagram

## 4 Method

### 4.1 Data collection

#### 4.1.1 Shape classification

The data for shape classification was collected using two prototypes (a) square bellow and (b) collapsible paper column as shown in Figure 14. Three different 3D printed structures of the material PLA (Polylactic acid) represented in Figure 15 are used to obtain images of 4 different shapes namely square, rectangle, circle and triangle. The images obtained with an endoscope from these incident shapes are shown in Figure 16. The camera captures images with a resolution of 640x480 pixels.

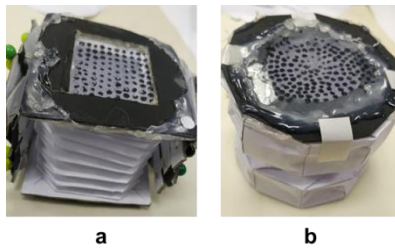


Figure 14: a) Bellow prototype, b) Paper column prototype

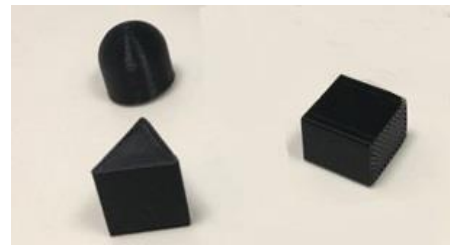


Figure 15: 3-D printed shapes

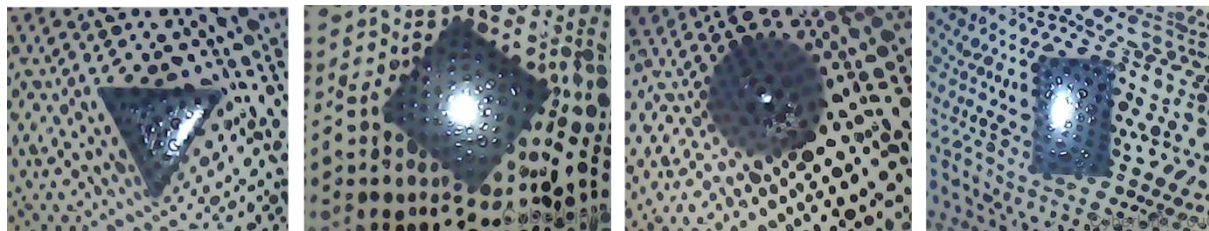


Figure 16: Shape classification images

#### 4.1.2 Force estimation

The data collection for force estimation is done with the Instron universal testing machine (UTM) which has a force testing capacity range from as low as 0.02N to as high as 50kN. The data was captured using a load-cell with a capacity of 100N. The setup for this data collection is as represented in the Figure 17 with the force applied vertically on the object which is placed on top of the elastomeric material. The data is collected from the collapsible paper column prototype. The experiment was done such that different images were captured, at the same time taking down the absolute force values shown on the software. The data is collected from 13 different locations capturing images for 5 different values of force (0N, 0.1N, 0.2N, 0.3N, 0.5N) at each location. Figure 18 shows only one group.

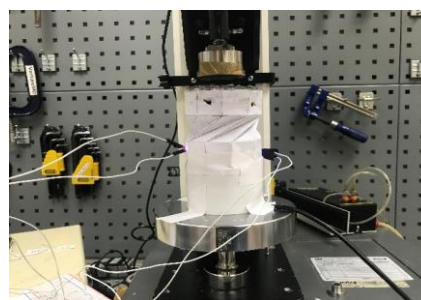


Figure 17: Setup of force estimation



Figure 18: Force estimation images

## 4.2 Data Processing

### 4.2.1 Shape classification

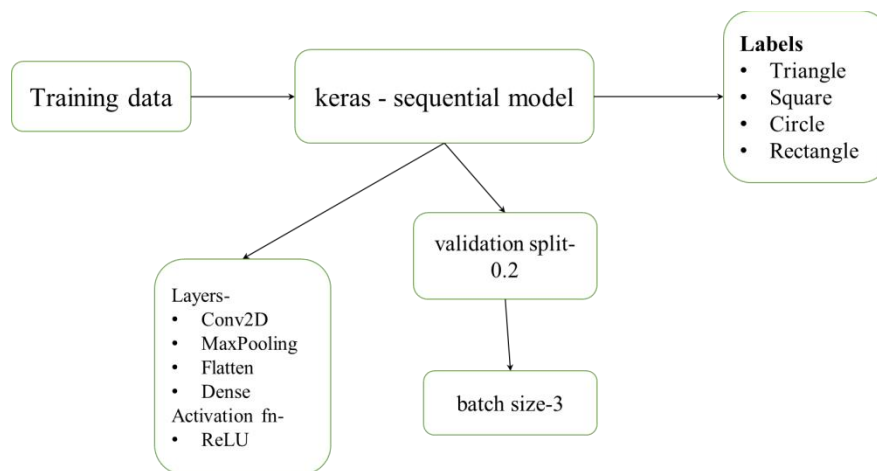


Figure 19: Algorithm for shape classification

A Convolutional Neural Network (CNN) model is used for Shape classification. A keras sequential model is used for image classification in the google Colab notebook for the classification of images. Two different training and validation data were used for the two different prototypes. The images used for the training of the modules are a set of six images captured at different depths from both the paper column prototype and the bellow prototype for the four different labels- square, circle, rectangle, triangle. A standard data set of shapes was also used from the Kaggle dataset of shapes for the square, circle, triangle shapes. For the previously unavailable dataset of the fourth shape of a rectangle, binary images of rectangles were created with open CV and used for training. Hence 100 standard images and 6 collected images were used for the training of the model making it 106 images per class. The model used was a 2D CNN sequential model generally used for classification of images[39]. The different layers of the model are Convolution 2D, MaxPooling 2D, Flatten, Dense, Dropout. The kernel size used for the convolution layers is 3x3 and the input shape is also defined. Finally, the model is compiled and

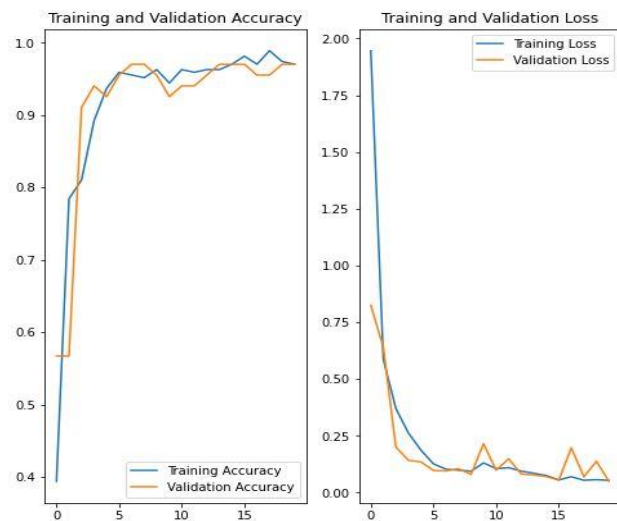


Figure 20: Graph of training and validation accuracy of Shape classification CNN model

trained to obtain a training and validation accuracy graph as represented in Figure 20 where the accuracy increases with the number of epochs and the loss decreases. Here, the shape of sample is classified into square, rectangle, triangle, and Circle.

#### 4.2.2 Force estimation

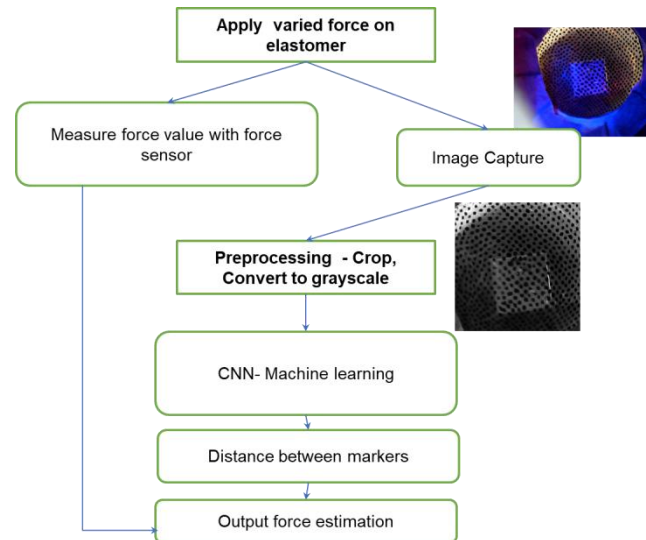


Figure 21: Algorithm for force estimation

The images are captured for 5 different classes of data with forces of 0N, 0.1N, 0.2N, 0.3N, 0.5N. These values of force are applied at 13 different locations capturing a total of 65 images. These images are used for training of the CNN keras sequential model. The data in this case are not augmented because the orientation of the markers changes which leads to inaccurate training of the model. The markers if drawn mechanically maintaining equal distance will be constant throughout the surface and the data can be augmented for better training and efficiency. The images are captured with illumination from 2 LED's on lateral edges, which could also lead to minimal variation in the intensity of the images during the data collection, to eradicate this error the images are pre-processed before training. The preprocessing involves cropping of the image to remove the area other than the sensor area and conversion to grayscale as indicated in the fig\_. After sufficient pre-processing, the model is assumed to be trained by the distance between the markers. The property of expansion in the marker field indicating the contact force applied serves as the main principle of force estimation[40]. After training the model, it is then validated with a 0.2 split in the data and the accuracy of training and validation is as shown in Figure 22. The figure shows fluctuations in the accuracy due to human error in marking of the elastomeric field and slight intensity variations which can be eradicated with further work.

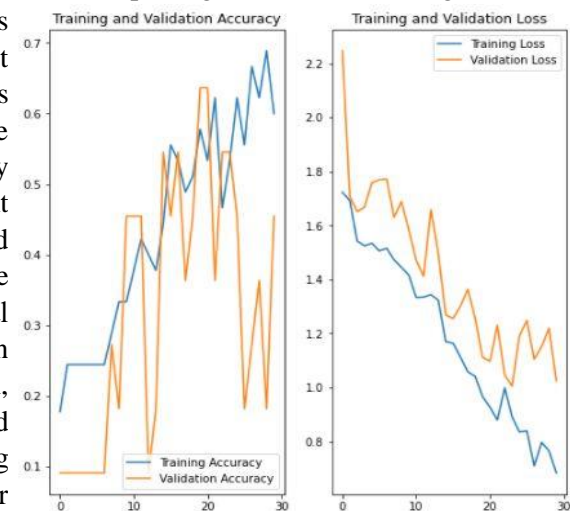


Figure 22: Graph of training and validation accuracy of Force classification CNN model



## 4 Results

In this project, two different origami structures, i.e. square bellow and collapsible paper column, were compared. In [Section 3.3.2](#), theoretical calculation for degrees of freedom of 3-D origami structure indicated that due to more number of creases bellow structure would have more uncertainty in motion and hence would be more unstable as compared to the paper column structure. During the data collection process it was observed that controlling the bellow structure to obtain good quality images was more difficult. This also reflected the quality of data collected ([Figure 23](#)).



Figure 23: Shape classification data collected by bellow and paper column structures

Therefore, the preliminary shape data collected validates theoretical calculations.

Paper column structure has a better performance in terms of shape classification accuracy as well, as can be observed in [Figure 24](#). This could again be due to the better stability of the structure.

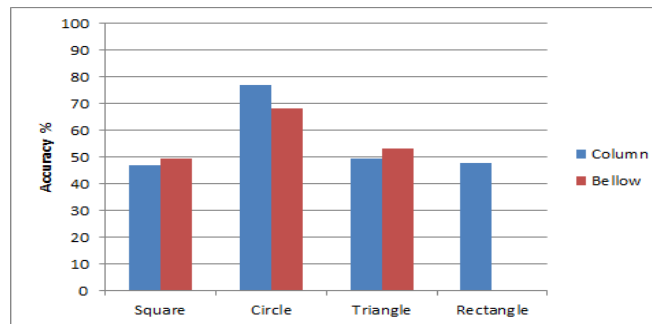


Figure 24: Shape classification accuracy of bellow and paper column for four shapes

Another important result is that the paper column structure shows bistability. The two stable states are:

- Fully stable closed (collapsed) state
- Partially stable open state which is stable till a force of 1N is applied, following which the structure collapses.

In real time applications the force applied can be increased with a sturdier prototype and hence can be used on tissues.

The experimentation shows that, for both the structures, the elastomeric membrane deforms when a force is applied to it, and marker field displacement is observed. From the output of the machine learning algorithm, we conclude that the model is able to obtain shape classification of 4 different structures and classify the force into 5 different classes.

Yi et al. has developed a hardness estimation model using shape classification and force estimation data for spherical shaped subject [13]. Appropriate mathematical models are required to be developed for hardness estimation of the other three shapes, i.e. triangle, square and rectangle. Thus, the results obtained from shape classification and force estimation can be eventually used for hardness estimation, which in turn can be used on tissues to add tactile capabilities to endoscopic shafts.

---

## 5 Conclusion

From the theoretical analysis in [Section 3.3.2](#) and results obtained, it can be concluded that in terms of accuracy and stability, the collapsible paper column is fundamentally better. The comparison between two types of illumination indicated better image capture with lateral illumination from LEDs of two different wavelengths to avoid the loss of marker patterns. The project hence provides a proof of concept of the use of flexible origami soft robotics in applications involving the tactile sensing which can be used in biomedical industries and also in other manufacturing industries by making a couple of changes to the Neural network models. The methodology currently used for shape classification and force estimation can also be further extended for obtaining other tactile properties.

## 6 Limitations and Future Work

The proposed design can have a major impact on improving the safety and effectiveness of the endoscopic surgical procedure. Currently, we have demonstrated the proof of concept using a paper model of dimensions in the cm scale. However, in the future, the structure can be miniaturized, as origami structure is size-invariant. Further, the material can be changed to a biocompatible and sturdier counterpart. Moreover, actuation can be added to advance the design into a fully functional robotic shaft. Some of the origami actuation mechanisms are discussed in [Table 4](#), which can be taken into consideration.

In the scope of this project, the marker field was drawn manually on the elastomeric membrane. However, there was an effort to place the markers on equal distances, but the process was prone to human error. Since position of the markers plays an important role in machine learning algorithm, this aspect requires improvement. In future, the process of placing markers can either be automated or off the shelf component can be used.

On the AI front, currently small number samples could be collected, which affected the accuracy of the machine learning algorithm. A larger dataset can be used to achieve better machine learning accuracy.

In this project we have demonstrated shape classification and force estimation. These two parameters can be implemented with an appropriate mathematical model to obtain hardness and other tactile properties of the structure. Yi et al. has achieved hardness estimation for spherical objects [13]. Although the project focused on endoscopic minimally invasive surgery, there are many other applications which can utilize the proposed concept. As illustrated in [41] and [42] origami structures are used in a lot of navigational robotics applications. The concept proposed in this project can be used to add tactile sensing capabilities to these robots. Thus, the can go a long way by adding an additional sense to the robot to a range of applications like disaster management, manufacturing, agriculture etc.

## References

- [1] A. Hamed *et al.*, “Advances in Haptics, Tactile Sensing, and Manipulation for Robot-Assisted Minimally Invasive Surgery, Noninvasive Surgery, and Diagnosis,” *Journal of Robotics*, Dec. 31, 2012. <https://www.hindawi.com/journals/jr/2012/412816/> (accessed Sep. 22, 2020).
- [2] O. A. J. van der Meijden and M. P. Schijven, “The value of haptic feedback in conventional and robot-assisted minimal invasive surgery and virtual reality training: a current review,” *Surg. Endosc.*, vol. 23, no. 6, pp. 1180–1190, Jun. 2009, doi: 10.1007/s00464-008-0298-x.
- [3] “Endoscopy of the pancreatic duct: value of different endoscope types - ScienceDirect.” <https://www.sciencedirect.com/science/article/abs/pii/S0016510793701078> (accessed Sep. 23, 2020).
- [4] Jun Ueda, Y. Ishida, M. Kondo, and T. Ogasawara, “Development of the NAIST-Hand with Vision-based Tactile Fingertip Sensor,” in *Proceedings of the 2005 IEEE International Conference on Robotics and Automation*, Barcelona, Spain, 2005, pp. 2332–2337, doi: 10.1109/ROBOT.2005.1570461.
- [5] A. Yamamoto, S. Nagasawa, H. Yamamoto, and T. Higuchi, “Electrostatic tactile display with thin film slider and its application to tactile telepresentation systems,” *IEEE Trans. Vis. Comput. Graph.*, vol. 12, no. 2, pp. 168–177, Mar. 2006, doi: 10.1109/TVCG.2006.28.
- [6] S. Okamoto, M. Konyo, Y. Mukaibo, T. Maeno, and S. Tadokoro, “Real-time Estimation of Touch Feeling Factors Using Human Finger Mimetic Tactile Sensors,” in *2006 IEEE/RSJ International Conference on Intelligent Robots and Systems*, Beijing, China, Oct. 2006, pp. 3581–3586, doi: 10.1109/IROS.2006.281648.
- [7] “(PDF) A tactile sensor for measuring hardness of soft tissue with applications to minimally invasive surgery,” *ResearchGate*. [https://www.researchgate.net/publication/319619121\\_A\\_tactile\\_sensor\\_for\\_measuring\\_hardness\\_of\\_soft\\_tissue\\_with\\_applications\\_to\\_minimally\\_invasive\\_surgery](https://www.researchgate.net/publication/319619121_A_tactile_sensor_for_measuring_hardness_of_soft_tissue_with_applications_to_minimally_invasive_surgery) (accessed Sep. 23, 2020).
- [8] S. Zhao, D. Parks, and C. Liu, “Design and modeling of a wide dynamic-range hardness sensor for biological tissue assessment,” *IEEE Sens. J.*, vol. 13, no. 12, pp. 4613–4620, Oct. 2013, doi: 10.1109/JSEN.2013.2271736.
- [9] M. Lambeta *et al.*, “DIGIT: A Novel Design for a Low-Cost Compact High-Resolution Tactile Sensor with Application to In-Hand Manipulation,” *IEEE Robot. Autom. Lett.*, vol. 5, no. 3, pp. 3838–3845, Jul. 2020, doi: 10.1109/LRA.2020.2977257.
- [10] C. D. Onal, R. J. Wood, and D. Rus, “An origami-inspired approach to worm robots,” *IeeeAsme Trans. Mechatron.*, vol. 18, no. 2, pp. 430–438, 2013.
- [11] E. Peraza Hernandez, D. Hartl, R. Malak, and D. Lagoudas, “Origami-inspired active structures: A synthesis and review,” *Smart Mater. Struct.*, vol. 23, p. 094001, Aug. 2014, doi: 10.1088/0964-1726/23/9/094001.
- [12] W. Yuan, M. A. Srinivasan, and E. H. Adelson, “Estimating object hardness with a GelSight touch sensor,” in *2016 IEEE/RSJ International Conference on Intelligent Robots and Systems (IROS)*, Daejeon, South Korea, Oct. 2016, pp. 208–215, doi: 10.1109/IROS.2016.7759057.
- [13] L. J. Yi, L. Seenivasan, and K. Kumar, “Deep Learning Based Depth Mapping, Classification And Force Estimation For Haptic Vision,” p. 15.
- [14] A. Eklund, A. Bergh, and O. A. Lindahl, “A catheter tactile sensor for measuring hardness of



soft tissue: measurement in a silicone model and in anin vitro human prostate model,” *Med. Biol. Eng. Comput.*, vol. 37, no. 5, pp. 618–624, Sep. 1999, doi: 10.1007/BF02513357.

[15] A. Gillman, G. Wilson, K. Fuchi, D. Hartl, A. Pankonien, and P. Buskohl, “Design of Soft Origami Mechanisms with Targeted Symmetries,” *Actuators*, vol. 8, no. 1, Art. no. 1, Mar. 2019, doi: 10.3390/act8010003.

[16] J. Butler, “Highly Compressible Origami Bellows for Harsh Environments,” *Theses Diss.*, Nov. 2017, [Online]. Available: <https://scholarsarchive.byu.edu/etd/6657>.

[17] A. A. Abtan, “Design and Fabrication of Origami Elements for use in a Folding Robot Structure,” phd, University of Leeds, 2019.

[18] K. Lee, Y. Wang, and C. Zheng, “TWISTER Hand: Underactuated Robotic Gripper Inspired by Origami Twisted Tower,” *IEEE Trans. Robot.*, vol. 36, no. 2, pp. 488–500, Apr. 2020, doi: 10.1109/TRO.2019.2956870.

[19] A. A. Abtan, “Design and Fabrication of Origami Elements for use in a Folding Robot Structure,” p. 160.

[20] Y. Chen, J. Yan, and J. Feng, “Geometric and Kinematic Analyses and Novel Characteristics of Origami-Inspired Structures,” *Symmetry*, vol. 11, no. 9, Art. no. 9, Sep. 2019, doi: 10.3390/sym11091101.

[21] J. Butler *et al.*, “Highly Compressible Origami Bellows for Harsh Environments,” in *Volume 5B: 40th Mechanisms and Robotics Conference*, Charlotte, North Carolina, USA, Aug. 2016, p. V05BT07A001, doi: 10.1115/DETC2016-59060.

[22] “origami water bomb - Grasshopper.” <https://www.grasshopper3d.com/photo/origami-water-bomb/prev?context=use> (accessed Sep. 23, 2020).

[23] “Symmetry | Free Full-Text | Geometric and Kinematic Analyses and Novel Characteristics of Origami-Inspired Structures.” <https://www.mdpi.com/2073-8994/11/9/1101> (accessed Sep. 23, 2020).

[24] “TWISTER Hand: Underactuated Robotic Gripper inspired by Origami Twisted Tower.” <https://art.engr.tamu.edu/publication/twister-hand-underactuated-robotic-gripper-inspired-by-origami-twisted-tower/> (accessed Sep. 23, 2020).

[25] R. V. Martinez, C. R. Fish, X. Chen, and G. M. Whitesides, “Elastomeric Origami: Programmable Paper-Elastomer Composites as Pneumatic Actuators,” *Adv. Funct. Mater.*, vol. 22, no. 7, pp. 1376–1384, Apr. 2012, doi: 10.1002/adfm.201102978.

[26] L. Paez, G. Agarwal, and J. Paik, “Design and Analysis of a Soft Pneumatic Actuator with Origami Shell Reinforcement,” 2016. /paper/Design-and-Analysis-of-a-Soft-Pneumatic-Actuator-Paez-Agarwal/26832dc37dab021a4c61c90e2496d6c7c65bfca8 (accessed Nov. 08, 2020).

[27] J. Koh, S. Kim, and K. Cho, “Self-Folding Origami Using Torsion Shape Memory Alloy Wire Actuators,” presented at the ASME 2014 International Design Engineering Technical Conferences and Computers and Information in Engineering Conference, Jan. 2015, doi: 10.1115/DETC2014-34822.

[28] K. Kuribayashi *et al.*, “Self-deployable origami stent grafts as a biomedical application of Ni-rich TiNi shape memory alloy foil,” *Mater. Sci. Eng. Struct. Mater. Prop. Microstruct. Process.*, vol. 419, no. 1–2, pp. 131–137, 2006.

[29] S. Miyashita *et al.*, “Folding Angle Regulation by Curved Crease Design for Self-Assembling

Origami Propellers,” *J. Mech. Robot.*, vol. 7, no. 2, May 2015, doi: 10.1115/1.4029548.

[30] “Origami Robot: A Self-Folding Paper Robot With an Electrothermal Actuator Created by Printing - IEEE Journals & Magazine.” <https://ieeexplore-ieee-org.libproxy1.nus.edu.sg/document/7519030> (accessed Nov. 08, 2020).

[31] M. Piñeirua, J. Bico, and B. Roman, “Capillary origami controlled by an electric field,” *Soft Matter*, vol. 6, no. 18, pp. 4491–4496, Sep. 2010, doi: 10.1039/C0SM00004C.

[32] J. Ryu, M. D’Amato, X. Cui, K. N. Long, H. Jerry Qi, and M. L. Dunn, “Photo-origami—Bending and folding polymers with light,” *Appl. Phys. Lett.*, vol. 100, no. 16, p. 161908, Apr. 2012, doi: 10.1063/1.3700719.

[33] J. M. Zanardi Ocampo *et al.*, “Characterization of GaAs-based micro-origami mirrors by optical actuation,” *Microelectron. Eng.*, vol. 73–74, pp. 429–434, Jun. 2004, doi: 10.1016/j.mee.2004.03.012.

[34] K. Kuribayashi-Shigetomi, H. Onoe, and S. Takeuchi, “Cell Origami: Self-Folding of Three-Dimensional Cell-Laden Microstructures Driven by Cell Traction Force,” *PLoS ONE*, vol. 7, no. 12, p. e51085, Dec. 2012, doi: 10.1371/journal.pone.0051085.

[35] “Origami Simulator.” <https://origamisimulator.org/> (accessed Nov. 06, 2020).

[36] A. Ghassaei, E. D. Demaine, and N. Gershenfeld, “Fast, Interactive Origami Simulation using GPU Computation,” p. 16.

[37] Y. Zhao, Y. Kanamori, and J. Mitani, “Design and motion analysis of axisymmetric 3D origami with generic six-crease bases,” *Comput. Aided Geom. Des.*, vol. 59, pp. 86–97, Jan. 2018, doi: 10.1016/j.cagd.2017.10.002.

[38] T. Tachi, “Geometric Considerations for the Design of Rigid Origami Structures,” p. 12, 2010.

[39] H. A. Atabay, “BINARY SHAPE CLASSIFICATION USING CONVOLUTIONAL NEURAL NETWORKS,” 2017. /paper/BINARY-SHAPE-CLASSIFICATION-USING-CONVOLUTIONAL-Atabay/293f18ca52946de3af8d8919deeea97786c6419c (accessed Nov. 11, 2020).

[40] T. Assaf, C. Roke, J. Rossiter, T. Pipe, and C. Melhuish, “Seeing by Touch: Evaluation of a Soft Biologically-Inspired Artificial Fingertip in Real-Time Active Touch,” *Sensors*, vol. 14, no. 2, Art. no. 2, Feb. 2014, doi: 10.3390/s140202561.

[41] T. Manwell, B. Guo, J. Back, and H. Liu, “Bioinspired setae for soft worm robot locomotion,” *2018 IEEE Int. Conf. Soft Robot. RoboSoft*, 2018, doi: 10.1109/ROBOSOFT.2018.8404896.

[42] A. Pagano, T. Yan, B. Chien, A. Wissa, and S. Tawfick, “A crawling robot driven by multi-stable origami,” *Smart Mater. Struct.*, vol. 26, no. 9, p. 094007, Sep. 2017, doi: 10.1088/1361-665X/aa721e.